Effects of Cost Structure in Optimal Control on Biological Arm Movement: A Simulation Study

Yuki Ueyama

Department of Rehabilitation Engineering
Research Institute of National Rehabilitation Center for Persons with Disabilities
4-1 Namiki, Tokorozawa, Saitama 359-8555, Japan
ueyama-yuki@rehab.go.jp

Abstract. We have to choose muscle activation pairs of agonist and antagonist muscles from a variety of combinations to achieve a movement. Even though there is a redundancy problem, we could immediately solve the problem and generate movements with a characteristic muscle activation pattern that the muscle pairs burst alternatively as the biphasic or triphasic shape. In this paper, in order to investigate requirements that derive the muscle activation pattern, we carried out numerical simulations of arm movement using a musculoskeletal arm model and an approximately optimal feedback control law with changing the cost structure. As a result, the muscle activation pattern could be reproduced by the simulation with a cost form composed by four terms, i.e., position, velocity, force and energy consumption. Thus, the muscle activations may correspond to cost terms. Furthermore, we suggest that the brain also regulate the force as well as the spatial accuracy and efficiency in the absence of any force interaction.

Keywords: Motor control, Reaching, Cost function, Muscle, Monkey.

1 Introduction

A biological motor system consists of many joints and muscles, forming a redundant system with multiple dimensions of freedom. The central nervous system (CNS) has to solve some redundancy problems, e.g., determining a movement trajectory and a pattern of muscle activity consisting of pairs of agonist and antagonist muscles. Besides, it was reported that the muscle activation pattern is equivalent to other movements loaded by an external force when the movements are kinematically same and the dynamics is well learned even if the amount of muscle activations is increased [1]. The typical pattern has been found that the agonist and antagonist muscles burst alternatively as the biphasic or triphasic pattern of muscle activation in single-joint reaching movements [2]. In addition, we also observed the muscle activation pattern in multi-joint movements in a monkey [3]. However, it has been suggested that most of motor control and planning models (i.e., the minimum jerk model and other criterions) could not predict a specific muscle action, e.g., a muscle co-contraction depending on tasks [4-6].

M. Lee et al. (Eds.): ICONIP 2013, Part I, LNCS 8226, pp. 241–248, 2013.

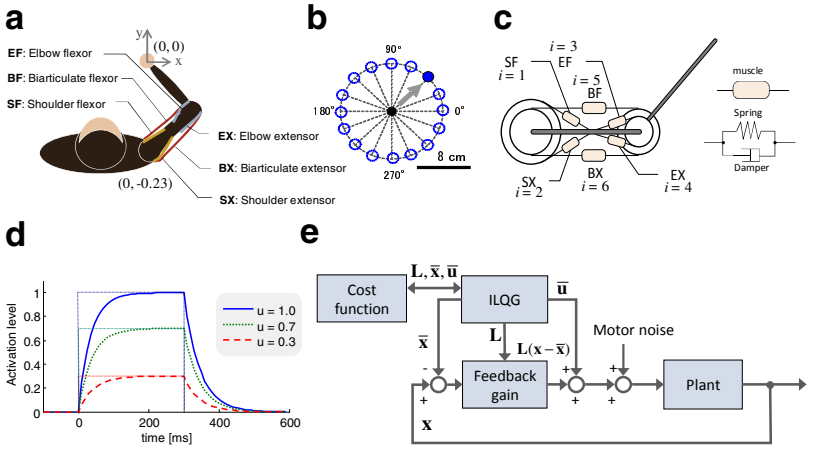

Fig. 1. Simulation model. (a) Setup of the center-out reaching task. The start position is 23-cm forward away from the round axis of the shoulder. (b) Reaching targets of the task. The targets are aligned as an 8-cm radial circle around the start position. (c) 2-link 6-muscle arm model. (d) Muscle activation dynamics. (e) Block diagram of the ILQG optimal control law.

Recently, optimal feedback control (OFC) theory has been proposed [7], and it is a plausible control model that could solve the redundancy problem. In addition, the theory could predict variability of movement phenomena [4, 5, 8]. In neural studies, it also has been suggested that primary motor cortex provides a neural substrate for integrating shoulder and elbow motion information into joint torque for fast feedback control [9].

In this study, we applied the iterative linear-quadratic-Gaussian (ILQG) method [10], which is an approximately OFC, to the biological arm dynamics and examined a role of cost structure formed by kinetic terms in order to investigate a source of the muscle activation pattern. As a result, the OFC could selectively coordinate muscles according to the movement direction, and an interlaced cost of the terminal position, velocity, force, and the entire energy consumption could induce similar activation patterns reported in previous studies [2, 3]. Consequently, we suggest that the brain may control the body according to an OFC mechanism adapting a cost function composed at least the four terms.

2 Methods

We simulated arm movements for a center-out reaching task using the iterative linear-quadratic-Gaussian (ILQG) method [10] and a 2-joint 6-muscle arm model (Fig.1a-c). The ILQG method constructs an affine feedback control law by minimizing a quadratic approximation to optimize a cost function, and could predict dynamic stiffness during arm movement [8].

2.1 The Two-Joint Six-Muscle Arm Model

We considered the monkey's arm to be a two-joint arm that was composed of the shoulder and elbow joints (Fig.1a). The joint variables were calculated in accordance with the kinematics of the monkey, and the joint angles were defined as a vector, $\boldsymbol{\theta} = [\theta_{sh}, \theta_{el}]^T$. The subscripts '*sh*' and '*el*' represent the shoulder and elbow variables, respectively. Thus, the dynamics of the monkey's arm in horizontal space is denoted by

$$\mathbf{M}(\boldsymbol{\theta})\ddot{\boldsymbol{\theta}} + \mathbf{C}(\boldsymbol{\theta}, \dot{\boldsymbol{\theta}}) = \boldsymbol{\tau}, \tag{1}$$

where $\boldsymbol{\tau} \in R^2$ corresponds to the joint torque vector. $\mathbf{M}(\boldsymbol{\theta}) \in R^{2\times 2}$, $\mathbf{C}(\boldsymbol{\theta}, \dot{\boldsymbol{\theta}}) \in R^2$ are the inertia matrix, the coriolis vector, respectively, and are represented by the link parameters, i.e., mass m_i, length l_i, distance from the joint center of the mass l_{gi}, and moment of inertia I_i (i = 1: upper arm, i = 2: forearm).

Although there are a large number of muscles that act on the arm in the horizontal plane, we have modeled only two degrees of freedom actuated by six muscle groups: elbow flexors (EF), elbow extensors (EX), shoulder flexors (SF), shoulder extensors (SX), biarticulate flexors (BF), and biarticulate extensors (BX) (Fig.1c). The joint torque is a function of its moment arms $\mathbf{A} \in R^{2\times 6}$ and the muscle tension $\mathbf{T} \in R^6$, and it is given by $\boldsymbol{\tau} = \mathbf{A} \cdot \mathbf{T}$. The moment arm is defined as the perpendicular distance from the muscle's line of action to the joint's center of rotation, given by

$$\mathbf{A} = \begin{bmatrix} \alpha_{11} & -\alpha_{12} & 0 & 0 & \alpha_{15} & -\alpha_{16} \\ 0 & 0 & \alpha_{23} & -\alpha_{24} & \alpha_{25} & -\alpha_{26} \end{bmatrix}.$$

Here, we used the Kelvin-Voigt model, consisting of an elastic element for static isometric contraction. The jth muscle tension T_j (j = 1, 2, …, 6) is determined from the muscle activation a_j and muscle length $L_j(\boldsymbol{\theta})$, and muscle-contraction velocity $V_j(\dot{\boldsymbol{\theta}}) = -dL_j(\boldsymbol{\theta})/dt$, according to the formula;

$$\begin{cases} T_j^{cmd} = K_j(a_j) \cdot \left[L_j(\boldsymbol{\theta}) - L_j^{rest}(a_j) \right]_+, & [\cdot]_+ := \max\{\cdot, 0\}, \\ T_j = T_j^{cmd} - B_j(a_j) \cdot V_j(\dot{\boldsymbol{\theta}}) \end{cases} \tag{2}$$

where $K_j(a_j)$, $B_j(a_j)$, and $L_j^{rest}(a_j)$ are the muscle elasticity, viscosity, and resting length, respectively. T_j^{cmd} is the active contraction force that must be generated as a positive value, similar to actual muscles, to generate the commanded torque with the moment arms. The values of muscle parameter in equation (2) are determined from the muscle activation as

$$K_j(a_j) = k^0 + k^1 a_j, \quad B_j(a_j) = b^0 + b^1 a_j, \quad L_j^{rest}(a_j) = L_j^{rest0} - L^{rest1} a_j, \tag{3}$$

where k^0, b^0 and L_j^{rest0} are the intrinsic elasticity, viscosity, and resting length of the *j*th muscle, respectively, and k^1, b^1 and L^{rest1} represent the variation in elasticity, viscosity, and resting length depending on the muscle activation, respectively. L_j^{rest0} was set to the muscle length at an optimal joint angle that allowed the muscle to generate maximal force. Note that, since constant components of the muscle length do not affect the arm dynamics, the muscle length vector $\mathbf{L}(\boldsymbol{\theta}) \in R^6$ could be denoted in a simplistic form by $\mathbf{L}(\boldsymbol{\theta}) \approx -\mathbf{A}^T\boldsymbol{\theta}$.

The muscle activation a_j is not equal to the instantaneous neural input u_j, but is generated by passing u_j thorough a filter that describes the calcium dynamics modeled with a first-order non-linear filter (Fig.1d) as

$$\dot{a}_j = \frac{(1+\sigma_u\varepsilon)u_j - a_j}{t(u_j, a_j)}, \text{ with } t(u_j, a_j) = \begin{cases} t_{deact} + u_j(t_{act} - t_{deact}) & u_j > a_j \\ t_{deact} & otherwise \end{cases}.$$

The input-dependent activation dynamics are faster than the constant deactivation dynamics. Thus, they were set as t_{act} = 40 [ms], t_{deacct} = 50 [ms].

The parameters required for the model are provided in Table 1-3.

2.2 Approximately Optimal Feedback Control

We transformed the 2-joint 6-muscle model into a state-space model. The control object was denoted by the state variable $\mathbf{x} = \begin{bmatrix} \boldsymbol{\theta}^T & \dot{\boldsymbol{\theta}}^T & \boldsymbol{\tau}_{cmd}^T & \mathbf{a}^T \end{bmatrix}^T$, where $\mathbf{a} \in R^6$ is the muscle activations, and $\boldsymbol{\tau}_{cmd} \in R^2$ is commanded torques which are removed the muscle viscosity component from the actual torques [11]. Using non-linear functions $F(\mathbf{x})$ and $G(\mathbf{x})$, the dynamics of the 2-joint 6-muscle arm model at time step t could be written into a state-space equation described as $\mathbf{x}_{t+1} = F(\mathbf{x}_t) + G(\mathbf{x}_t)\cdot(\mathbf{I} + \boldsymbol{\sigma}_\mathbf{u}\boldsymbol{\varepsilon}_t)\mathbf{u}_t$. Note that the non-linear functions $F(\mathbf{x})$ and $G(\mathbf{x})$ are defined just for a descriptive purpose to represent the dynamics in an affine form. In practice, they were given as locally linearized forms around each state at time t to obtain an approximately OFC law. Neural input $\mathbf{u}_t$ is disturbed by a signal-dependent, multiplicative noise that exists in the neural system [12]. The signal-dependent noise is given by $\boldsymbol{\varepsilon}_t$, a zero-mean Gaussian white noise with unity covariance ($\boldsymbol{\varepsilon}_t \in R^2$ is a vector). The magnitude of the signal-dependent noise was set by the scaling parameter $\boldsymbol{\sigma}_\mathbf{u}$ ($\boldsymbol{\sigma}_\mathbf{u}$ = 0.2 in this study).

Table 1. Link parameters

		l_i [m]	l_{gi} [m]	m_i [kg]	I_i [kg m^2]
Upper arm	(i = 1)	0.15	0.075	0.5	3.8×10^{-3}
Forearm	(i = 2)	0.21	0.12	0.5	9.1×10^{-3}

Table 2. Moment arms and optimal joint angles

Muscle	Moment arm α_{ij} [cm]		Optimal joint angle [deg]	
	$i = 1$	$i = 2$	$i = 1$	$i = 2$
$j = 1$	2.6	-	45	-
$j = 2$	1.3	-	15	-
$j = 3$	-	1.2	-	90
$j = 4$	-	1.7	-	110
$j = 5$	0.7	1.6	45	100
$j = 6$	2.5	1.1	15	100

Table 3. Muscle parameters

L^{rest1} [m]	k^0 [N m^{-1}]	k^1 [N m^{-1}]	b^0 [(N·s) m^{-1}]	b^1 [(N·s) m^{-1}]
0.02	50	30,000	2.5	300

The approximately OFC law for ILQG is given by $\mathbf{u}_t = \bar{\mathbf{u}}_t + \mathbf{L}_t(\mathbf{x}_t - \bar{\mathbf{x}}_t)$, where $\bar{\mathbf{u}}_t$ is an open-loop control component, $\mathbf{L}_t$ is the feedback control gain, and $\bar{\mathbf{x}}_t$ is a nominal trajectory (Fig.1e). The parameters $\bar{\mathbf{u}}_t$, $\mathbf{L}_t$, and $\bar{\mathbf{x}}_t$ were computed iteratively using the Levenberg-Marquardt algorithm to optimize the following cost function;

$$J = \min_{\mathbf{u}(\cdot)} \Big[w_p \left\| \mathbf{p}(\boldsymbol{\theta}(T_f)) - \mathbf{p}^* \right\|^2 + w_v \left\| \dot{\mathbf{p}}(\boldsymbol{\theta}(T_f), \dot{\boldsymbol{\theta}}(T_f)) \right\|^2 + w_f \left\| \mathbf{F}_{cmd}(\boldsymbol{\theta}(T_f), \boldsymbol{\tau}_{cmd}(T_f)) \right\|^2 + \frac{1}{T_f} \int_0^{T_f} \left\| \mathbf{u} \right\|^2 dt \Big], \tag{4}$$

where $\mathbf{p}(\boldsymbol{\theta}(T_f))$, $\mathbf{F}_{cmd}(\boldsymbol{\theta}(T_f), \boldsymbol{\tau}_{cmd}(T_f))$ are the end-point position and commanded force which corresponds to the commanded torque, in Cartesian space at a terminal time T_f = 400 [ms]. They are given by the forward kinematics. Additionally, $\mathbf{p}^*$ is a target position in Cartesian space, and w_p, w_v, w_f are cost weights of the position, velocity, and force accuracies at the terminal state, respectively. On the right-hand side of equation (4), the first, second and third terms evaluate the end-point accuracy; the fourth term, which is the sum of the squares of the neural inputs during the movement, evaluates the effort cost.

2.3 Center-Out Reaching Movement

We examined a center-out reaching movement task in this study. The position of the movement start was set to a position 23 cm in front of the shoulder (Fig.1a), and 16 targets were aligned as an 8-cm radial circle around the start position (Fig.1b).

The simulations were carried out to make three cases of requirement of the movement manipulating the terminal cost weights (Table 4). In Case 1, the terminal cost weights were zero except the positional cost. This task corresponded a shooting

Table 4. Cost weight values

Cost weight		Case 1	Case 2	Case 3	Case 4
w_p	(Position)	1.0×10^3	1.0×10^3	1.0×10^3	1.0×10^4
w_v	(Velocity)	0	1.0×10^2	0	5.0×10^2
w_f	(Force)	0	0	5.0	1.0×10

task has the end-point passed the target. In Case 2, the terminal cost weight of the end-point force was zero. It required movements under kinematic constraints. In Case 3 required achieving a movement under kinetic constraints. The task ordered to regulate the end-point force to zero at the movement end. In other words, it was required to maintain the final position after the task.

An initial state of muscle activation levels was set to maintain the initial posture, (i.e., [x, y] = [0, 0]), as the joint torque was equal to zero. The simulations used simple Euler integration with 10 ms time step.

3 Results

The hand trajectories were varied slightly curved or nearly straight lines in accordance with the direction excepting Case 3 in which there were some trajectories changed the movement directions suddenly (Fig. 2c). In Case 1, the tangential velocities did not converge to zero at the movement end, and the joint torques were weakly generated at the movement onset. In Case 2, the velocities were to be zero. However, they were sometimes shaped trapezoidal form, and the torques were generated the opposite direction of the movements in order to break the speed. In Case 3, the velocities sometimes burst at the movement end, and the torques were drastically increased and converged to zero at the movement end. In Case 4, the velocities were closed to zero in gradual curves, and showed clear bell-shaped profiles. In addition, the negative and positive torques were changed alternatively, and converged to zero at the movement end.

Moreover, the muscle activities were also varied according to the cases. In Case 1, agonist muscles were activated once just after the movement start. In Case 2, agonist and antagonist muscles were activated alternatively at just after the movement start and the movement end, respectively. In Case 3, the muscles were activated once, however, the timing was divided into two patterns, i.e., after the movement onset or before the movement end. In Case 4, the muscles were activated once or twice. Especially to the SF and BX muscles, when they took a role as an agonist muscle, they were activated twice at the movement start and end. On the other hand, there were single activations at the middle time of the movement when they would be an antagonist muscle.

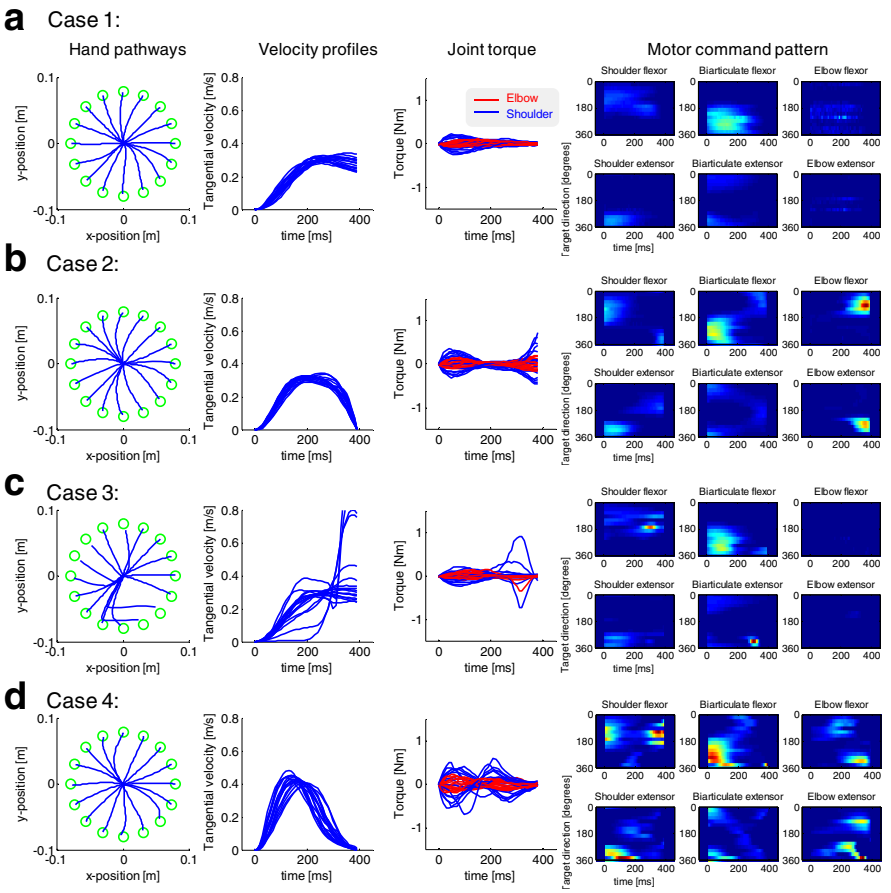

Fig. 2. Simulation results. Each row respectively shows hand pathways, velocity profiles, joint torque profiles, and motor command patterns from the left to right. In the rightmost row, the motor command patterns plotted as a function of time and target direction. Light color indicates high value and dark color indicates low value. The values are normalized by the highest activation level in each muscle across all cases. (a)-(d) respectively represent the Case 1–4.

4 Conclusion

We carried out numerical simulations of biological arm movement using an approximately OFC approach. Additionally, we adapted four types of cost structures in order to examine influences to motor behavior, i.e., kinematic trajectory and muscle activity. As a result, the positional cost made first agonist muscle activation to induce the movement. The velocity cost corresponded to the antagonist muscle activation to stop the movement. There were single-peaked pattern of motor command in the case of the cost function without the force term, and joint torques at terminal time was not converged to zero (Fig. 2). In contrast, a cost function with the

position and force terms was not sufficient to make a bell-shaped velocity curve. However, a cost structure including the position, velocity and force terms could generate diphasic motor command patterns, and the velocity and torque converged to zero at the terminal state similar to experimental measurements [2]. In this cost form, the force term induced the second agonist muscle activation to suppress an opposite torque generated by the antagonist muscle which was activated to reduce the movement speed. Furthermore, the muscles were activated selectively in accordance with the movement directions similar to previous studies. This result indicates that the OFC could coordinate muscles adequately according to the movement direction.

In conclusion, we suggest that the CNS may control the body according to an optimal control mechanism adapting a cost function regulating the force as well as the spatial accuracy and efficiency in the absence of any force interaction.

References

1. Darainy, M., Ostry, D.J.: Muscle cocontraction following dynamics learning. Exp. Brain Res. 190, 153–163 (2008)
2. Hallett, M., Shahani, B.T., Young, R.R.: EMG analysis of stereotyped voluntary movements in man. J. Neurol. Neurosurg. Psychiatry. 38, 1154–1162 (1975)
3. Ueyama, Y., Miyashita, E.: Devising a Robotic Arm Manipulandum for Normal and Altered Reaching Movements to Investigate Brain Mechanisms of Motor Control. Instrum. Sci. Technol. 41, 251–273 (2013)
4. Ueyama, Y., Miyashita, E.: Signal-Dependent Noise Induces Muscle Co-Contraction to Achieve Required Movement Accuracy: A Simulation Study with an Optimal Control. Curr. Bioinform. 8, 16–24 (2013)
5. Mitrovic, D., Klanke, S., Osu, R., Kawato, M., Vijayakumar, S.: A Computational Model of Limb Impedance Control Based on Principles of Internal Model Uncertainty. PLoS One 5, e13601 (2010)
6. Osu, R., Kamimura, N., Iwasaki, H., Nakano, E., Harris, C.M., Wada, Y., Kawato, M.: Optimal impedance control for task achievement in the presence of signal-dependent noise. J. Neurophysiol. 92, 1199–1215 (2004)
7. Todorov, E., Jordan, M.I.: Optimal feedback control as a theory of motor coordination. Nat. Neurosci. 5, 1226–1235 (2002)
8. Ueyama, Y., Miyashita, E.: Optimal Feedback Control for Predicting Dynamic Stiffness during Arm Movement. IEEE Trans. Ind. Electron. 61 (in press, 2014)
9. Pruszynski, J.A., Kurtzer, I., Nashed, J.Y., Omrani, M., Brouwer, B., Scott, S.H.: Primary motor cortex underlies multi-joint integration for fast feedback control. Nature 478, 387–390 (2011)
10. Li, W., Todorov, E.: Iterative linearization methods for approximately optimal control and estimation of non-linear stochastic system. Int. J. Contr. 80, 1439–1453 (2007)
11. Nakano, E., Imamizu, H., Osu, R., Uno, Y., Gomi, H., Yoshioka, T., Kawato, M.: Quantitative examinations of internal representations for arm trajectory planning: minimum commanded torque change model. J. Neurophysiol. 81, 2140–2155 (1999)
12. Harris, C.M., Wolpert, D.M.: Signal-dependent noise determines motor planning. Nature 394, 780–784 (1998)